

# HIGH RESOLUTION MOTION ESTIMATION OF SEA ICE USING AN IMPLICIT QUAD-TREE APPROACH

**M. Thomas,**

Video/Image Modeling and Synthesis Lab,  
Dept. of Comp. and Info. Sciences,  
University of Delaware,  
Newark, DE 19716

**C. A. Geiger,**

Center for Climatic Research,  
Dept. of Geography,  
University of Delaware,  
Newark, DE 19716

**C. Kambhamettu,**

Video/Image Modeling and Synthesis Lab,  
Dept. of Comp. and Info. Sciences,  
University of Delaware,  
Newark, DE 19716

**KEY WORDS:** RADARSAT, motion estimation, Quadtree decomposition, phase correlation, line integral convolution

## ABSTRACT:

In this paper we estimate the motion between time-lagged Synthetic Aperture Radar (SAR) image pairs via an implicit quad-tree scheme. The algorithm provides a means to estimate motion at a spatial resolution that is an order of magnitude greater than the currently available data products. Since the motion is extracted from the image data iteratively, the estimated field provides an accurate picture of the underlying discontinuous motion. Experimental tests indicate that the algorithm is also computationally efficient. This is extremely valuable when attempting to localize leads and ridges that are created in sea ice.

## 1 INTRODUCTION

The dynamics of heat variation on the surface of the Earth has been intimately connected with the thermal regulators of the planet - the polar icecaps. The formation and melting of the sea ice gives us an improved understanding of the dynamics that is taking place there. With the availability of 'high spatial resolution all-weather' Synthetic Aperture Radar (SAR) imagery, we now have an important component that could provide us with complementary information when observed in tandem with the *in situ* buoys.

Thus given a pair of time-lagged SAR images, the relative motion taking place between the two images would provide an indication of the non rigid dynamics that is taking place. This problem of estimating the relative displacement has been a significant area of research in computer vision since the work on optical flow by Horn and Schunck (Horn and Schunck, 1981). Since then there have been several variants that have been developed to tackle various difficulties in estimating the apparent motion. The readers are referred to (Barron et al., 1994) and the references therein, for a broader perspective of the computation of motion using the optic flow constraint. In typical high frame-rate imagery, the optic flow method has been applied to achieve impressive results. But when handling satellite imagery, the low temporal sampling rate (polar repeat rate of 1~3 days) tend to alias the nonrigid motion that might be occurring at a frequency higher than the repeat rate of the satellite. In addition to these difficulties, when analyzing large imagery (15000×15000 pixels), computational efficiency of the algorithm becomes a criterion that is as important as the robustness of the technique.

We have, in this work, made an attempt to tackle the above stated problems in a computationally efficient and robust manner via an implicit quad-tree decomposition scheme. We specifically consider remote sensed data to show the reliability of our mechanism but inherently this algorithm is general enough to warrant its application to other problems. With regards to the data set that was used for testing, the "Surface Heat Budget of the Arctic Ocean" (SHEBA) data set (Stern and Moritz, 2002) provide a valuable test bed to evaluate the robustness and accuracy of the algorithm.

The organization of the paper is as follows. We begin with a brief overview of the currently available techniques for motion estima-

tion and a description of the SHEBA data set. We subsequently describe the algorithm that we developed to tackle the observed motion. We then analyze the performance of the algorithm with real data sets having large discontinuous motion and finally conclude with possible future directions.

## 2 RELEVANT BACKGROUND

When analyzing satellite images, one of the biggest obstacle is that the high spatial resolution of satellite data is limited by its low temporal resolution. Under the influence of fast moving storms, significant non-linear changes in discontinuities can occur at temporal scales much lesser than 3 days. Within this duration, sea ice can deform rapidly resulting in large changes in the orientation, distribution, and size of continuous and discontinuous regions. The estimation of this deformation would thus require algorithms that can tackle these non linearities when computing the motion when compared to the traditional optical flow algorithms.

Traditional optic flow algorithms, (Horn and Schunck, 1981) and its variants, assume that the temporal resolution and the observed motion is relatively very small. Under this assumption, the optic flow equation is considered valid and many techniques have been developed to estimate the flow field (Lucas and Kanade, 1981), (Nagel and Enkelmann, 1986). Robust techniques (Black and Anandan, 1993), (Bab-Hadiashar and Suter, 1998), (Ong and Spann, 1999) have also emerged to handle the large noise and/or the failure of the underlying image motion model. But most of the above methods guarantee a plausible solution only when the observed motion is relatively small. In the presence of large motion, many of the techniques do not converge efficiently and/or accurately to a valid solution.

Within the field of sea ice, the problem of extracting the deformation using satellite images is addressed using a variety of methods including cross correlation (Kwok et al., 1990), (Liu and Cavalieri, 1998), (Kwok et al., 1998), (Drinkwater, 1998) and 2D wavelets (Fily and Rothrock, 1987). But unfortunately typical data products are computed at a very coarse resolution (lowest resolution is 5km), which provides a limited information of the underlying dynamics. In contrast, our algorithm attempts to estimate the motion at a resolution of ~400m, which is a magnitude greater than typically available data products. This estimate is

obtained directly from the image data without using any form of data interpolation. This high resolution estimate provides a means to accurately localize discontinuous regions and be able to visualize motion at close proximity to the discontinuities.

### 3 DATA DESCRIPTION

The Surface Heat Budget of the Arctic Ocean (SHEBA) camp was launched from October 1997 to October 1998. Coincident with the launch of the camp, the Canadian RADARSAT satellite collected 195 synthetic aperture radar (SAR) images of the camp site between the 1<sup>st</sup> of November 1997 and the 8<sup>th</sup> of October 1998. The images were captured using a C band (5.3 GHz) active microwave instrument. The swath of the satellite was 460 km leading to a pixel resolution of 50m with a polar repeat rate of  $\sim 1$ -3 days (Stern and Moritz, 2002). The images were collected at Alaska SAR facility in Fairbanks and were subsequently projected to the SSM/I polar stereographic projection (Drinkwater, 1998).

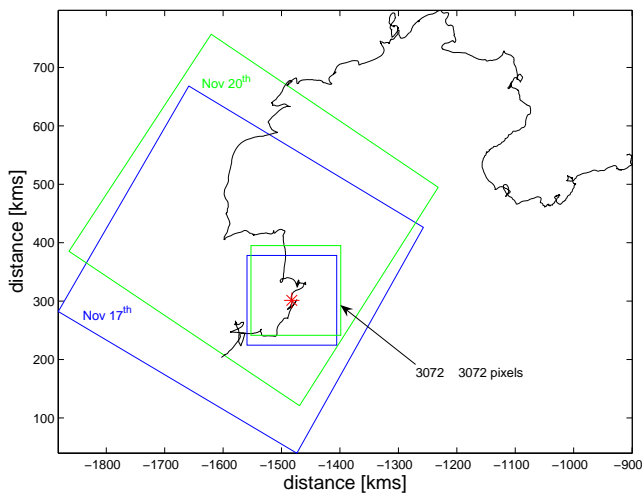


Figure 1: SHEBA camp shown in tandem with the bounding box of the satellite imagery in SSM/I.

The position of the SHEBA camp, in SSM/I stereographic projection, through the entire duration of time is shown in figure 1. The two large rectangular boxes are the bounding boxes of the actual images obtained from the satellite on the 17<sup>th</sup> and 20<sup>th</sup> of November, 1997. The asterisk indicates the position of the camp co-located with the satellite image on the 17<sup>th</sup>. The two inner rectangular boxes indicates an analysis window of 3072 $\times$ 3072 pixels, where the high resolution motion was estimated. The readers are referred to the Applied Physics Laboratory at the University of Washington, Seattle<sup>1</sup> for detailed information and data description of SHEBA camp.

### 4 DESCRIPTION OF THE ALGORITHM

It is essential to stress that unlike the typical motion estimation problem, here we used *in situ* buoy information to construct a Lagrangian Frame of Reference (LFR) to estimate the differential motion. Despite the use of *in situ* buoys as tie points, the differential motion that is typically observed between the image pair is still significantly large (figure 8(b)). The LFR is obtained by using the image time stamp to linearly interpolate the spatio-temporal position of the camp (GPS data from the camp available

<sup>1</sup><http://psc.apl.washington.edu/Harry/Radarsat/>

at 10 minutes intervals). Given this LFR for the image pair, the deformation can be subsequently estimated using our algorithm.

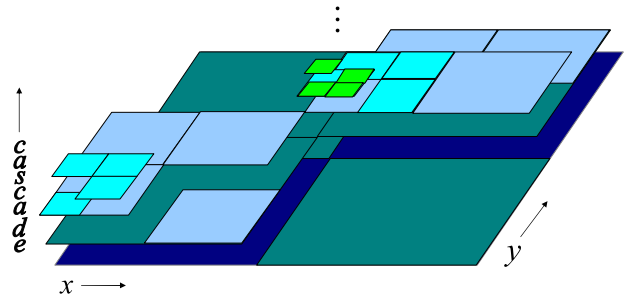


Figure 2: The quad-tree decomposition for the motion estimation.

To estimate the motion, we use a cascade of implicit quad-tree decompositions (Figure 2). Typically, a quad tree based algorithm requires the maintenance of a data structure to manage the various aspects of the tree linkage (Thomas et al., 2000). In our implementation, the decomposition occurs without an explicit data structure. The flow of information from the parent node to the child occurs due to the organization of the analysis modules and hence it can be perceived as an implicit quad-tree decomposition.

#### 4.1 Cascaded Motion Estimation

In our previous works (Thomas et al., 2004), (Thomas et al., 2005a), we have shown the efficacy of using phase correlation for estimating motion in ERS-1 imagery. But unlike the ERS-1 images, the motion that is observed in RADARSAT images involved extremely large discontinuous motion with basin-wide leads being observed. This type of dynamics indicate a quasi-rigid motion field (Kambhamettu et al., 1994) unlike the motion that is present in the ERS-1 imagery. To handle such quasi-rigid motion, we use the multi-scale motion estimation property of the quad tree decomposition.

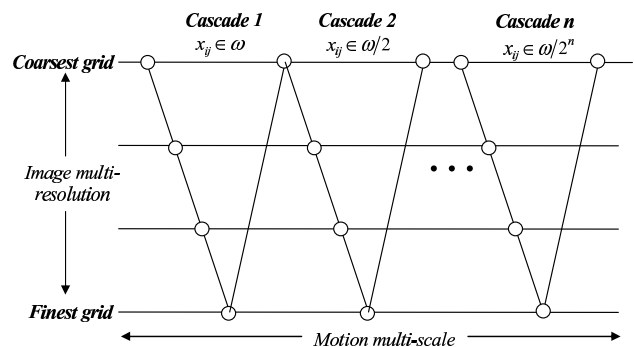


Figure 3: The “V-cycle” to perform the estimation-regularization-sampling cycle for robust estimation of motion.

To provide a better explanation of the quad decomposition, the estimation process can be compared with the full V-cycle method of multi-grid technique (Wesseling, 2004). This is shown in figure 3, where a circle indicates an estimation point and a diagonal line connecting any two circles indicate a data regularization step with up-sampling/down-sampling. Each V-cycle, thus denotes an estimation-regularization framework with the resolution of the flow field scaled by a factor of  $2^n$  at the  $n^{\text{th}}$  cascade. The main advantage of this mechanism is that the estimation at earlier stages of the cascade tend to be more robust, thereby directing subsequent estimation stages in the correct direction.

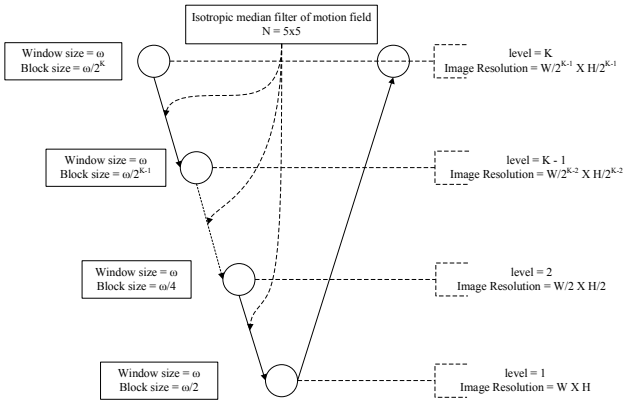


Figure 4: Data flow architecture within a cascade.

The data flow architecture within a cascade can be observed in figure 4. Two parameters that are used for the computation are the window size and the block size. The window size defines the dimension of the analysis window that is used to perform the phase correlation while the block size defines the sliding frequency. The block size provides a relationship of the overlap ratio between adjacent analysis windows. The smaller the block size, the greater the overlap between adjacent windows and vice versa. The minimum overlap of half the window size occurs at the finest level of the image resolution. The changing overlap ratio defines the smoothness of the estimated motion field with greater overlap leading to a smoother motion field.

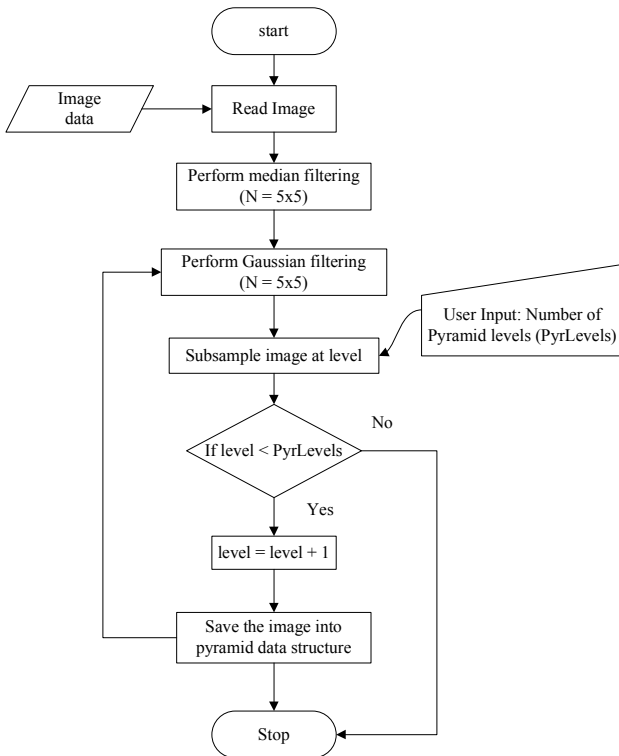


Figure 5: Flow chart for creating the multi resolution image pyramid.

As the cascade proceeds from the left to the right, the analysis window is reduced by half, thereby obtaining a more accurate representation of the dynamics taking place. This reduction in window size, decomposes the collocated analysis window in each cascade into four separate windows in the subsequent cas-

cade, thereby forming the quad tree decomposition. Since the estimate towards the left side is obtained by incorporating information from a larger area of the image, the motion tends to be more robust. But the decrease in the analysis windows tend to provide for a higher resolution of estimates towards the right. Thus each cascade builds on the robustness of its parent but performs the analysis at a resolution that is twice that of the parent. This provides a mechanism to transfer the robustness from left to right while simultaneously increasing the resolution of estimates.

## 4.2 Image Pyramid

As can be observed in figure 3, the horizontal lines indicate the various resolutions in an image hierarchy. The multi resolution image pyramid is computed as shown in the figure 5. The image pyramid is computed once at the beginning of the processing and is used for each stage of the cascade. This is possible because the algorithm does not warp the image data using the estimated vector field in the next estimation iteration. Instead the estimated motion from each cascade is accumulated leading to the final motion field.

## 4.3 Block Motion

Figure 6 shows the flow chart for the block motion estimation. Block similarity is computed using phase correlation and candidates are extracted from the phase correlation surface. The best candidate, from among the possible candidates, is selected using normalized cross correlation (NCC). This voting scheme improves the reliability of the estimated vectors over a single similarity metric alone. Phase correlation (Thomas, 1987), (Thomas et al., 2004) also has the advantage of being illumination invariant and can be efficiently estimated in the Fourier domain, unlike the Normalized Cross Correlation (Proakis and Manolakis, 1996), (Lewis, 1995). This allows the algorithm to be computationally very efficient.

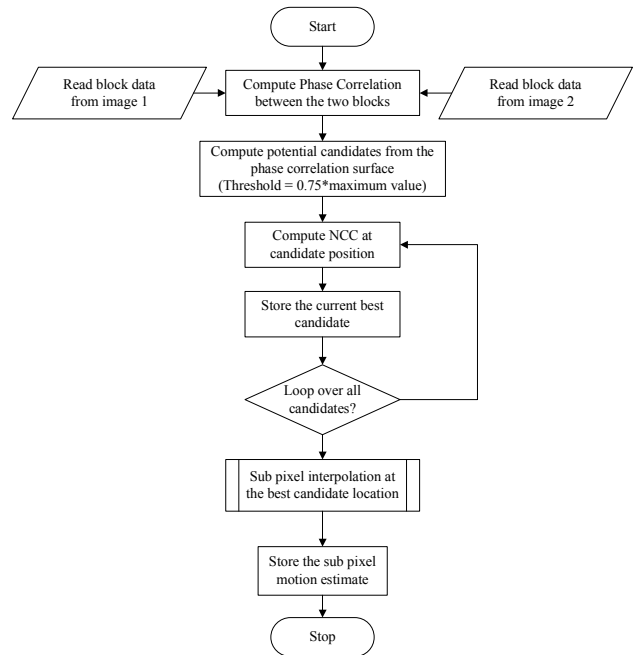


Figure 6: Flow chart for estimating local motion.

Once the best estimate is computed, subpixel motion is computed by using a 3-point Gaussian fit over the NCC values in the neighborhood of the best candidate (Thomas et al., 2005b).

## 5 RESULTS AND DISCUSSION

The estimation procedure was tested on two types of image pairs from the SHEBA data set. The first set constituted image pairs with a temporal difference of 1~3 days. These image pairs usually did not have significant discontinuities in them, and the pixel displacements were typically in the range of 0~100 pixels. The second was a simulated test case using image pairs with time-lag that were greater than 3 days. In these cases, there were significant damage zones with the typical motion in the range of 100~200 pixels. Figure 7 shows a sample image from the second test set. For the motion estimation algorithm, we used 4 cascades with 3 levels of image resolutions in each cascade. This led to an estimated motion field resolution of 400m when compared to the 5km SHEBA data product (Stern and Moritz, 2002). The algorithm was tested on 25 image pairs from the SHEBA data set and we have provided results from a few of the image pairs.

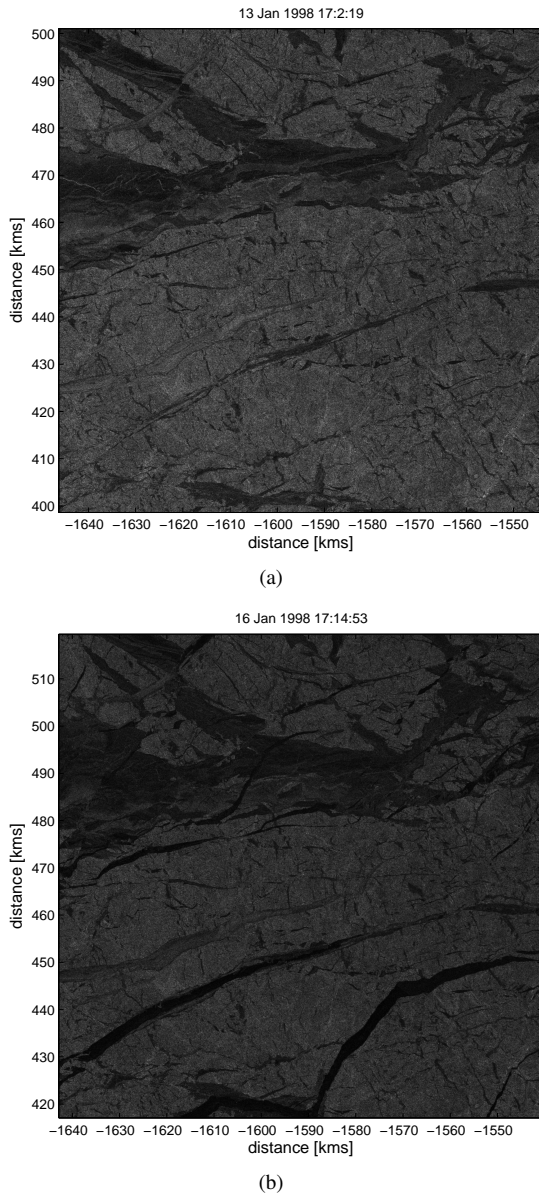


Figure 7: Image showing the second test case with extreme discontinuities (a) First image (b) Second Image.

In both the test cases, the motion estimation algorithm performed very well. For visualizing the flow field, we adopted the Line

Integral Convolution (LIC) as described by Cabral and Leedom (Cabral and Leedom, 1993). Figure 8 shows the advection of the streamlines of motion leading to the formation of the discontinuities<sup>2</sup>.

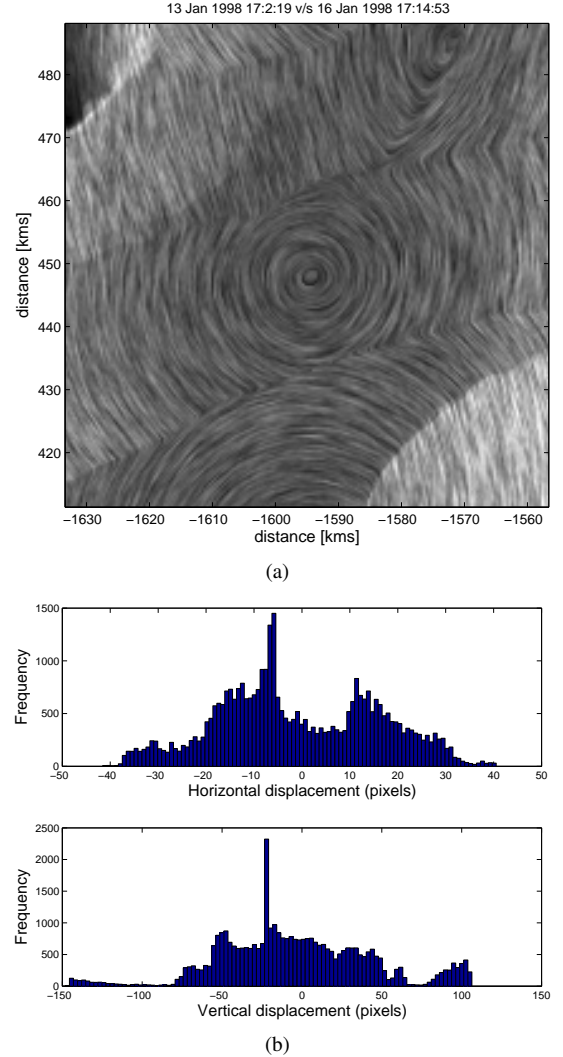


Figure 8: Image showing the test cases with extreme discontinuities (a) Motion estimated using our framework (b) Histogram of the displacement present in the images.

Further results can be seen in figure 9 and 10, where we have estimated the motion between image pairs with varying time differences. The LIC shows the estimated motion field, where coherent structures can be accurately observed, despite the presence of large discontinuities.

## 6 CONCLUSIONS AND FUTURE WORK

In this paper, we have described an estimation framework that has been found to be robust and computationally efficient. The noise robustness is achieved due to the implicit quad-tree scheme while the computational efficiency is achieved due to the Fourier computations that is present in the cascaded multi-scale approach. Our observations indicate that the algorithm can accurately estimate motion in the presence of large discontinuities. This would

<sup>2</sup>Line Integral convolution code was adapted from the work by W. Martin ([www.cs.utah.edu/~wmartin/cs523project/](http://www.cs.utah.edu/~wmartin/cs523project/))

be an extremely important component in understanding the dynamics that is taking place at the polar icecaps from satellite imagery

### ACKNOWLEDGEMENTS

The SAR imagery was provided through the Alaska SAR Facility through agreements with the ©Canadian Space Agency (1997) for use of their RADARSAT-1 imagery. Efforts leading to these results were originally supported through grants from the Office of Naval Research (N00014-03-1-0045 and N00014-02-1-0244) and continues to advanced through support of the National Science Foundation (NSF) Office of Polar Programs (OPP0612105).

### REFERENCES

- Bab-Hadiashar, A. and Suter, D., 1998. Robust total least squares based optic flow computation. In: ACCV, pp. 566–573.
- Barron, J., Fleet, D. and Beauchemin, S., 1994. Performance of optical flow techniques. *Int. J. Comp. Vision* 12(1), pp. 43–77.
- Black, M. and Anandan, P., 1993. A framework for the robust estimation of optical flow. In: *Proceedings of IEEE Computer Society International Conference on Computer Vision*, pp. 231–236.
- Cabral, B. and Leedom, L. C., 1993. Imaging vector fields using line integral convolution. In: *Proc. of 20th conference on Comp. graphics and interactive tech.*, pp. 263–270.
- Drinkwater, M., 1998. Analysis of SAR Data of the Polar Oceans. Springer-Verlag, chapter Satellite microwave radar observations of Antarctic sea ice, pp. 145–187.
- Fily, M. and Rothrock, D. A., 1987. Sea-ice tracking by nested correlations. *IEEE Trans. Geosci. Remote Sens.* GE-25(5), pp. 570–580.
- Horn, B. and Schunck, B., 1981. Determining optical flow. *Artificial Intelligence* 17, pp. 185–203.
- Kambhamettu, C., Goldgof, D., Terzopoulos, D. and Huang, T., 1994. Nonrigid motion analysis. In: *Handbook of Pattern Recognition and Image Processing: Computer Vision*, pp. 405–430.
- Kwok, R., Curlander, J. C., McConnell, R. and Pang, S., 1990. An ice motion tracking system at the alaska SAR facility. *IEEE J. Oceanic Eng.* 15(1), pp. 44–54.
- Kwok, R., Schweiger, A., Rothrock, D. A., Pang, S. and Kottmeier, C., 1998. Sea-ice motion from satellite passive microwave imagery assessed with ERS,SAR and buoy motions. *Journal of Geophysical Research* 103 (C4), pp. 8191–8214.
- Lewis, J., 1995. Fast normalized cross-correlation. In: *Vision Interface, Canadian Image Processing and Pattern Recognition Society*, pp. 120–123.
- Liu, A. K. and Cavalieri, D. J., 1998. On sea-ice drift from the wavelet analysis of the defense meteorological satellite program (DMSP) special sensor microwave imager (SSM/I) data. *Int. J. Remote Sens.* 19(7), pp. 1415–1423.
- Lucas, B. D. and Kanade, T., 1981. An iterative image registration technique with an application to stereo vision. In: *Proceedings of Image Understanding Workshop*, pp. 121–130.
- Nagel, H.-H. and Enkelmann, W., 1986. An investigation of smoothness constraints for the estimation of displacement vector fields from image sequences. *IEEE Trans. Pattern Anal. Mach. Intell.* 8, pp. 565–593.
- Ong, E. P. and Spann, M., 1999. Robust optical flow computation based on least-median-of-squares regression. *Int. J. Comp. Vision* 31(1), pp. 51–82.
- Proakis, J. G. and Manolakis, D. G., 1996. *Digital Signal Processing: Principles, Algorithms, and Applications*. Prentice Hall.
- Stern, H. L. and Moritz, R. E., 2002. Sea ice kinematics and surface properties from radarsat synthetic aperture radar during the sheba drift. *J. Geophys. Res.*
- Thomas, G. A., 1987. Television motion measurement for datv and other applications. Technical report, BBC Research Department.
- Thomas, M., Geiger, C. A. and Kambhamettu, C., 2004. Discontinuous non-rigid motion analysis of sea ice using c-band synthetic aperture radar satellite imagery. In: *IEEE Workshop on Articulated and Nonrigid Motion (ANM)*.
- Thomas, M., Geiger, C. A. and Kambhamettu, C., 2005a. Mesoscale sea ice features derived from discontinuous nonrigid motion sar products. In: *18th International Conference on Port and Ocean Engineering Under Arctic Conditions*.
- Thomas, M., Misra, S., Kambhamettu, C. and Kirby, J. T., 2005b. A robust motion estimation algorithm for piv. *Measurement Science and Technology* 16(3), pp. 865–877.
- Thomas, M. V., Shah, A. and Reddy, G. C., 2000. A fast block motion estimation algorithm based on motion adaptive partitioning. In: *Proc. Indian Conf. on Comp. Vis., Graphics and Image Proc. (ICVGIP)*.
- Wesseling, P., 2004. *An Introduction to Multigrid Methods*. R. T. Edwards.

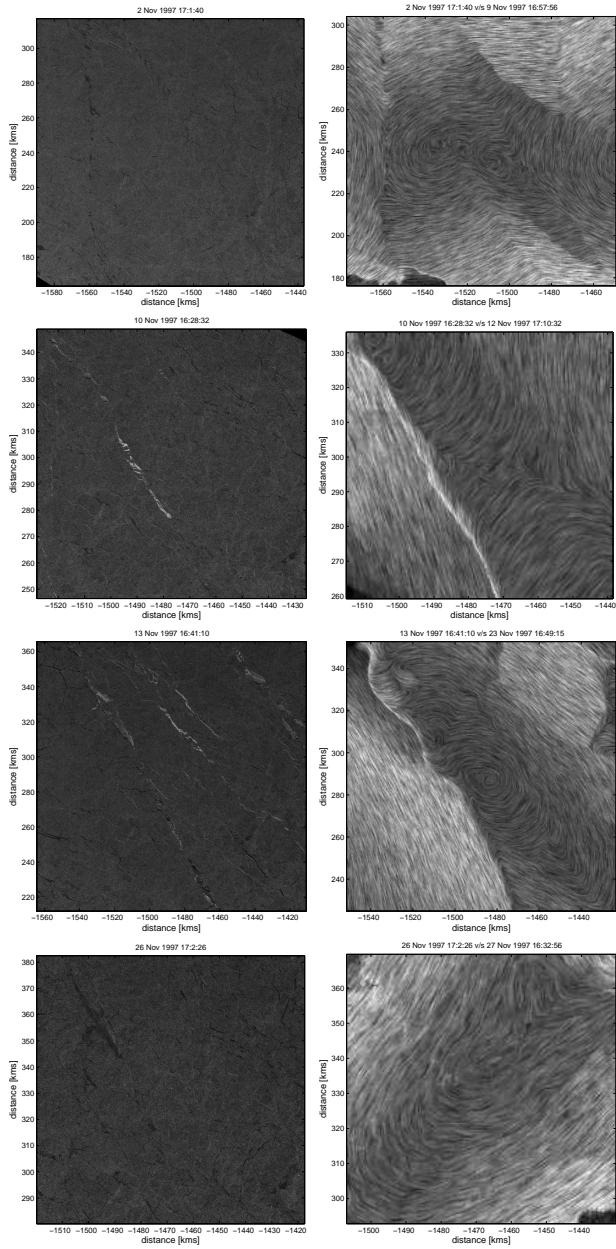


Figure 9: Results from high resolution motion estimation using sample image pairs at different time-lagged intervals. Only the first image is shown (left column) and the LIC of the estimated motion (right column).

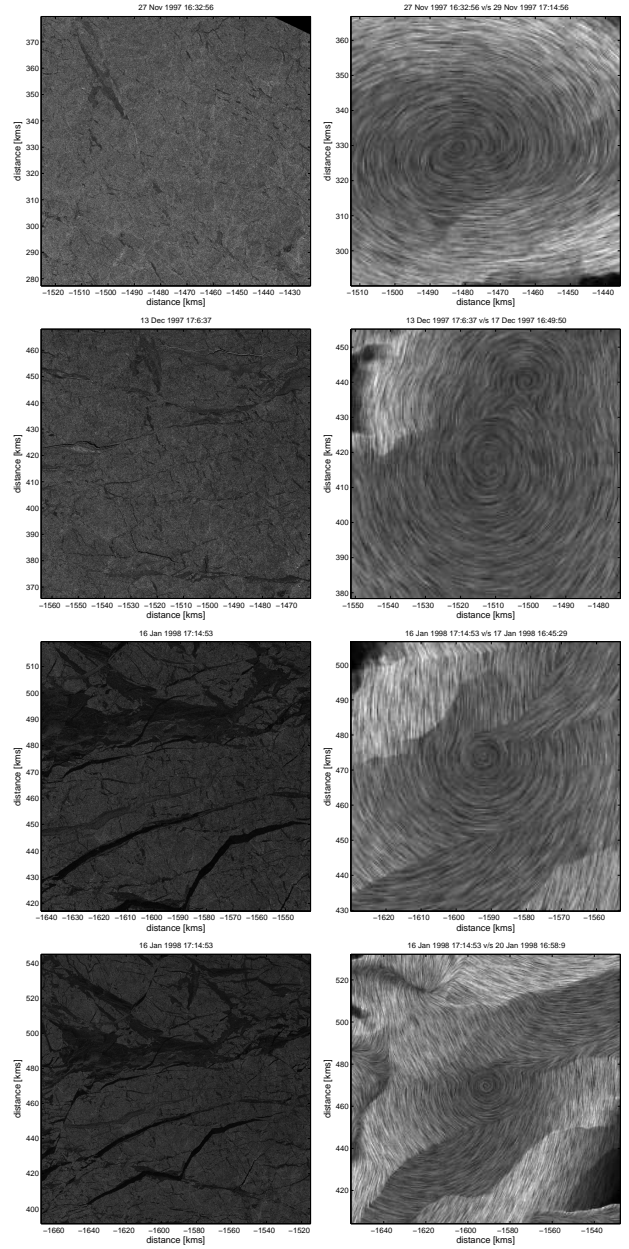


Figure 10: Results from high resolution motion estimation using sample image pairs at different time-lagged intervals. Only the first image is shown (left column) and the LIC of the estimated motion (right column).